

# ***Ab initio* density functional calculations of ferromagnetism in low-dimensional nanostructures: From nanowires to nanorods**

Martin Zelený,<sup>1</sup> Mojmir Šob,<sup>2,3</sup> and Jürgen Hafner<sup>1</sup>

<sup>1</sup>Center for Computational Materials Science and Faculty of Physics, University of Vienna, Sensengasse 8/12, A-1090 Wien, Austria

<sup>2</sup>Institute of Chemistry, Masaryk University, CZ-611 37 Brno, Czech Republic

<sup>3</sup>Institute of Physics of Materials, Academy of Sciences of the Czech Republic, CZ-611 62 Brno, Czech Republic

(Received 19 November 2008; revised manuscript received 12 January 2009; published 16 April 2009)

We present *ab initio* spin-density functional calculations of the electronic and magnetic properties of Fe and Ni nanostructures with a geometry varying between a straight linear wire and a three-dimensional nanorod. With decreasing tension along the axis of the nanostructure we find a series of transitions first from dimerized to periodic and zigzag wires, then to a planar triangular stripe, and further to a nanorod consisting of a periodic stacking of triangular antiprims. In all nanostructures atoms are in a high-moment state, with magnetic moments of about  $3.1\mu_B$  for Fe and about  $1\mu_B$  for Ni. A transition to a low-spin or nonmagnetic state is initiated at a fixed critical value of the interatomic distance, independent of dimension and coordination number. The analysis of the electronic structure shows that already for the one-dimensional nanostructures the ratio between exchange splitting and magnetic moment is close to the universal value  $I=\Delta/M\sim 1\text{ eV}/\mu_B$  established for bulk itinerant magnets.

DOI: 10.1103/PhysRevB.79.134421

PACS number(s): 64.70.Nd, 73.22.-f, 75.75.+a, 81.07.Vb

## I. INTRODUCTION

The magnetism of nanostructured materials is an exciting and timely field of research, stimulated by the interest in novel fundamental physics and by many potential applications. Much effort has been spent on the investigation of the influence of the dimensionality on the magnetic properties of nanostructures. The properties of one-dimensional (1D) (or quasi-one-dimensional) systems are particularly interesting. On one hand, it is well known that the reduced coordination of magnetic atoms in nanostructures leads to the formation of strongly enhanced magnetic moments, on the other hand the analysis of the properties of an isotropic Heisenberg model has demonstrated that a strictly one-dimensional chain of magnetic atoms does not order at any finite temperature.<sup>1</sup> However, even straight monoatomic chains suspended in space are not strictly one dimension due to the lateral extension of the electronic orbitals and the magnetic shape anisotropy. In practice, arrays of magnetic monoatomic nanowires may be produced by adsorbing atoms along the step edges of vicinal surfaces of nonmagnetic substrates.<sup>2</sup> In this case the weak coupling between wires mediated by the support and the magnetic anisotropy lead to an essentially two-dimensional (2D) characteristics of the magnetic ordering transition. For example, for arrays of monoatomic wires of Fe atoms supported at the step edges of vicinal Cu surfaces, it has been shown that the critical behavior is consistent with that of a two-dimensional anisotropic *XY* ferromagnet.<sup>3</sup> Both the strength of the interwire coupling and the anisotropy promote magnetic ordering at finite temperature.

Short nanowires have also been prepared by driving the tip of a scanning tunneling microscope (STM) into a metallic substrate and extrusion of a small number of atoms from either tip or surface upon retraction<sup>4–6</sup> or in mechanical break junctions.<sup>7–10</sup> Depending on the strain on the wire, the atoms will assume different configurations ranging from linear chains over zigzag chains to two-dimensional stripes and

three-dimensional (3D) rods. Electrochemical methods can be used to prepare nanostructures of different shapes and diameters varying between nanowires and nanotubes.<sup>11,12</sup> Nanowires have also been produced by encapsulation in carbon nanotubes.<sup>13,14</sup>

Most theoretical investigations of the magnetic properties of nanowires have been restricted to straight linear chains.<sup>3,15–18</sup> Studies allowing also for a zigzag geometry were first performed by Sanchez-Portal *et al.*<sup>19</sup> For Au wires it was shown that the ground-state configuration consists of a planar stripe of nearly equilateral triangles, in agreement with the experiments of Onishi *et al.*<sup>4</sup> and Yanson *et al.*<sup>5</sup> on wires drawn between two Au STM tips. Zigzag equilibrium configurations were also established for nanowires consisting of Cu atoms, simple metals (K, Ca, and Al),<sup>19–21</sup> and transition metals [Pd, Rh, and Ru,<sup>21</sup> Zr,<sup>22</sup> and Ti (Ref. 23)]. Recently Tung and Guo<sup>24</sup> performed a comparative investigation of linear and zigzag nanowires of all *3d* metals in nonmagnetic, ferromagnetic, and antiferromagnetic states. It was shown that for most metals, magnetism favors a zigzag equilibrium configuration. The structural energy difference is large (up to 1 eV/atom) for the ferromagnetic *3d*-metals Fe, Co, and Ni but much smaller for the antiferromagnetic metals Cr and Mn. For a zigzag Mn chain, ferromagnetic and antiferromagnetic states are energetically almost degenerate. For Ti and V the ground state is ferromagnetic for a linear but nonmagnetic for a zigzag chain. This demonstrates a strong correlation between the geometric and magnetic structures of nanowires. Very similar studies of periodic and finite chains and stripes of transition metals have also been published by Ataca *et al.*<sup>25</sup>

Magnetic nanowires formed by Fe, Co, and Ni encapsulated in single-wall nanotubes have very recently been studied by Jo and Lee.<sup>26</sup> For the nanowire a square profile with zigzag Fe chains on each of the faces has been assumed, with a periodicity along the axis matching that of the nanotube. The magnetic moment of the wire is found to depend on the

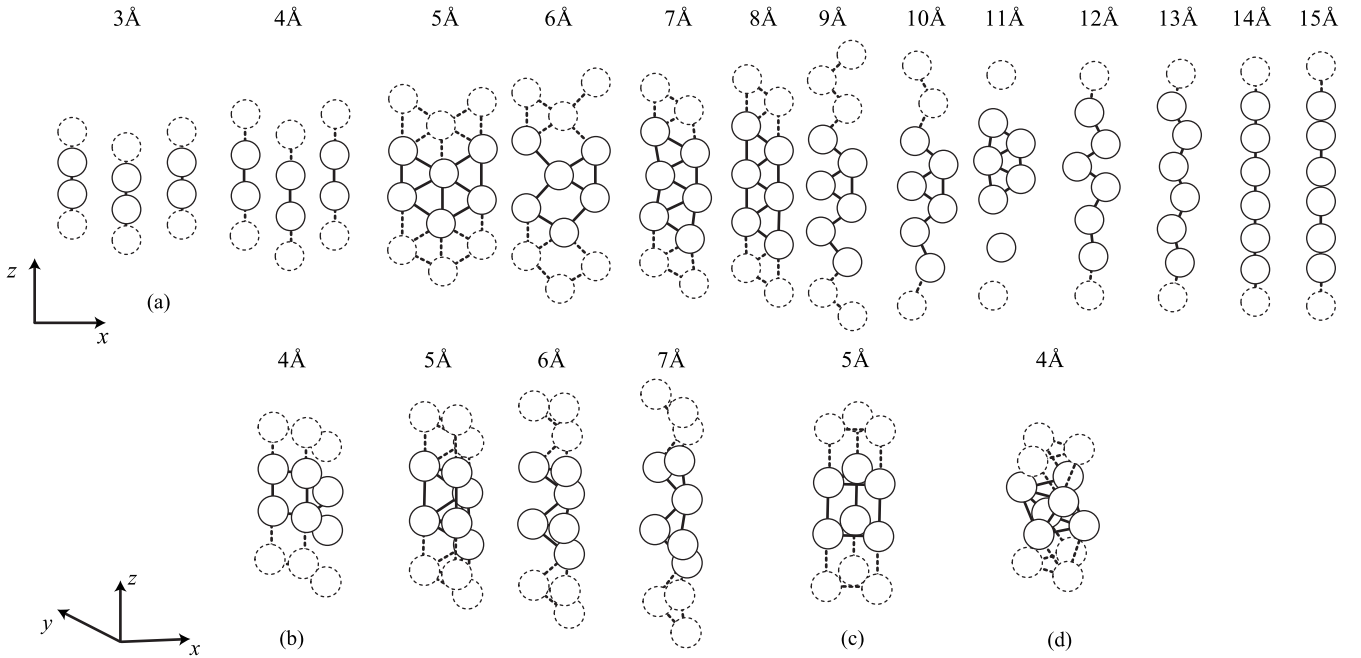


FIG. 1. Variation in the geometric structures as a function of the length of the unit cell under (a) two- and (b) three-dimensional relaxations. The (c) prismatic and (d) antiprismatic rods considered for comparison are also shown.

diameter of the nanotube; it is lower than in freestanding wires for a wire tightly wrapped in a tube with small diameter but may be even enhanced in loosely wrapped wires.

However, a consistent picture of the variation in the magnetic properties with a geometry changing gradually from one to three dimensions is missing. The present work is devoted to *ab initio* density functional investigations of the magnetic properties in low-dimensional nanostructures of Fe and Ni, ranging from monoatomic wires over two-dimensional stripes to three-dimensional rods.

## II. COMPUTATIONAL SETUP

The quantum-mechanical framework of our investigations is spin-density functional theory within the semilocal generalized-gradient approximation (GGA). We have used the Vienna *ab-initio* simulation package (VASP) (Ref. 27) which performs an iterative solution of the Kohn-Sham equations for periodic boundary conditions in a plane-wave basis. The basis set contained plane waves with kinetic energies up to 280 eV. The electron-ion interaction was described by projector-augmented wave (PAW) potentials.<sup>28,29</sup> The PAW approach shares the computational efficiency of the pseudopotential approach but is an all-electron technique avoiding the problems related to the linearization of the core-valence exchange interaction (this is particularly important for magnetic calculations). We use the gradient-corrected exchange-correlation functional proposed by Perdew, Burke, and Ernzerhof (PBE).<sup>30</sup> The use of the generalized-gradient approximation is essential for a correct description of the structural and magnetic ground state of Fe.<sup>31</sup> Using the PBE functional we calculate for body-centered-cubic (bcc) ferromagnetic Fe a lattice parameter of  $a_{\text{bcc}}=2.832$  Å (atomic volume  $\Omega=11.362$  Å<sup>3</sup>), a bulk modulus of  $B=1.66$  Mbar,

and a magnetic moment of  $M=2.20\mu_B$ . The corresponding experimental values are  $a_{\text{bcc}}=2.867$  Å,  $B=1.68$  Mbar, and  $M=2.22\mu_B$ .<sup>32</sup> For fcc Ni the calculated values are  $a_{\text{fcc}}=3.522$  Å,  $B=1.96$  Mbar, and  $M=0.63\mu_B$ , to be compared with  $a_{\text{fcc}}=3.524$  Å,  $B=1.86$  Mbar, and  $M=0.61\mu_B$  from experiment.<sup>32</sup>

Nanostructures are modeled by an ensemble of six atoms in a periodically repeated tetragonal cells with lateral dimensions along the  $x$  and  $y$  axes of 17 Å. The axis of the nanostructures (wire, stripe, or rod) is oriented along the  $z$  direction; tension or compression on the nanostructure was simulated by changing the height of the cell. Relaxation of the atomic structure was performed via a conjugate-gradient method using the exact Hellmann-Feynman forces acting on the atoms. Integration over the Brillouin zone was based on 12 special  $\vec{k}$  points. Convergence with respect to the number of  $k$  points has been tested and it was found that a set of 12 special points leads already to well-converged results. A straight monoatomic wire was produced by restricting relaxation to changes in the  $z$  coordinates of the atoms. Two-dimensional stripes are generated by permitting relaxation in a plane passing through the axis of the wire, while either imposing equal interatomic distances along  $z$  (“ $xy$  relaxed”) or allowing a full independent relaxation of five atoms in three directions, imposing only the periodic boundary conditions fixed by the cell size. The position of the sixth atom is fixed in the center of the basis of the cell. Figure 1 shows schematically the change in the atomic geometry of the nanostructures as a function of the length of the unit cell for two- and three-dimensional relaxations. If the atoms are constrained to remain within a plane, we observe with decreasing tension a transition from a straight to a zigzag wire, the formation of stripes based on triangular motifs, and finally under compressive strain the disintegration into separated

parallel wires. If relaxation in all three Cartesian directions is permitted, a transition to nanorods is observed. For comparison we include also nanorods formed by a periodic stacking of trigonal prisms or antiprisms which are not spontaneously formed upon compression of the cell. These two structures are relaxed only in a plane perpendicular to the axis, while the distance between the triangular base and top is fixed by the periodic boundary conditions.

The analysis of the magnetic structures has concentrated on collinear ferromagnetic configurations. For Ni this is in no way a restriction, but for Fe this requires some comment. bcc Fe is ferromagnetic, but for fcc Fe the magnetic ground state is known to be an incommensurate spin spiral which is slightly different from that defining a layered antiferromagnetic structure.<sup>33,34</sup> This raises the question whether for the Fe nanostructures noncollinear magnetic structures have to be taken into consideration. The magnetic order in Fe monowires has been investigated by Spišák and Hafner.<sup>3</sup> A large magnetic energy difference of 0.35 eV/atom favoring a collinear ferromagnetic relative to an antiferromagnetic state has been found. For ultrathin Fe layers epitaxially grown on Cu(100) substrate, Qian *et al.*<sup>35</sup> discussed the possible formation of a spin-density wave. A detailed investigation of possible noncollinear magnetic ordering in this system has been performed by Spišák and Hafner.<sup>36</sup> It was shown that up to a thickness of 4 monolayers, the Fe films are collinear ferromagnetic. On the basis of this evidence, the present study has concentrated on ferromagnetic Fe nanostructures.

### III. IRON NANOSTRUCTURES

The binding energies (defined relative to the isolated atoms), nearest-neighbor distances, and average magnetic moments for the local equilibrium configurations of nanostructure in one to three dimensions (from monoatomic wires to antiprismatic nanorods) shown in Fig. 1 have been compiled in Table I. These results already display some interesting trends. Under increasing compression, the atomic configuration changes in such a way that the nearest-neighbor distance remains approximately constant ( $d \sim 2.31 \pm 0.05$  Å), i.e., considerably lower than in bulk bcc Fe ( $d = 2.45$  Å). All nanostructures are in a high-moment state, the average magnetic moment decreasing slowly with increasing dimensionality (increasing coordination), from  $3.13\mu_B$  for a monowire to  $2.75\mu_B$  in an antiprismatic nanorod. These values span the same range as the magnetic moments calculated for the open Fe(100) ( $M = 3.05\mu_B$ ) and the close-packed Fe(110) ( $M = 2.74\mu_B$ ) surfaces of bcc Fe.<sup>37</sup> In the following paragraphs we will discuss details of the structural, magnetic, and electronic properties of the nanostructures and of the transformations between the various configurations.

#### A. Wires and stripes

We start our simulations from a 1D monoatomic chain with equal interatomic distances. Minimization of the total energy with respect to the height  $c$  of the cell yields an equilibrium bond length of  $d = 2.269$  Å ( $c = 13.611$  Å), in good agreement with the previously published results.<sup>3</sup> This

TABLE I. Binding energy  $E_B$  (eV/atom), cell height  $c$  (Å), nearest-neighbor distances  $d$  (Å), and average magnetic moment  $\bar{M}$  ( $\mu_B$ ) of Fe and Ni nanostructures calculated at local equilibrium.

	$E_B$	$c$	$d$	$\bar{M}$
Fe				
Monoatomic wire	-1.869	13.611	2.269	3.13
Triangular stripe	-2.857	7.594	2.235	2.92
Hexagonal stripe	-3.072	4.730	2.365	2.84
Prismatic rod	-3.063	4.963	2.268	2.91
Tetrahedral rod	-3.261	4.863	2.275	2.87
Antiprismatic rod	-3.578	3.864	2.310	2.75
Bulk bcc Fe			2.45	2.20
Ni				
Monoatomic wire	-2.027	13.086	2.181	1.11
Triangular stripe	-2.778	6.916	2.305	0.92
Hexagonal stripe	-3.108	4.702	2.317	0.88
Prismatic rod	-3.124	4.567	2.232	0.80
Tetrahedral rod	-3.211	4.675	2.266	0.80
Antiprismatic rod	-3.322	4.076	2.223	0.85
Bulk fcc Ni			2.49	0.63

value is somewhat smaller than the theoretical equilibrium nearest-neighbor distance in bcc iron of 2.453 Å. At the equilibrium distance the magnetic moment of the atoms in the chain is  $3.13\mu_B$ , i.e., substantially larger than the magnetic moment of bcc iron ( $2.20\mu_B$ ), due to the reduced coordination number in the linear chain.

Figure 2(a) shows the total energy of one- and two-dimensional Fe nanostructures as a function of the height of the periodically repeated cell; Fig. 2(b) shows the corresponding variations in the magnetic moments. Under tensile strain, a dimerization of the chain, introducing alternating short and long distances, is energetically favorable. A careful analysis shows that already at average distances only slightly larger than the equilibrium spacing of the straight monowire ( $d = 2.311$  Å), a dimerization with short and long bonds of  $(1 \pm 0.117) \times d$  leads to a slight reduction in the energy by about 19 meV/atom. Under increasing tension, dimerization becomes increasingly preferred, and the difference between short and long bonds increases. The length of the short bonds approaches the equilibrium bond length in a free Fe<sub>2</sub> dimer (theory: 2.02 Å; experiment: 2.03 Å, as reported by Moroni *et al.*<sup>31</sup>). Due to the short distances in the Fe<sub>2</sub> pairs, this leads to a slight reduction in the magnetic moments. Compressive strain leads to a rapid increase in the total energy and a strong reduction in magnetism; for the straight monowire a high-spin to low-spin transition starts at  $c \sim 12.5$  Å ( $d = 2.08$  Å).

In the range  $7.0 \text{ Å} \leq c \leq 13.5 \text{ Å}$  the formation of a zigzag chain, gradually transforming to triangular stripes, allows to lower the total energy. The energy minimum for a periodic triangular stripe is found at  $c = 7.594$  Å. The interatomic distance along the  $z$  direction is 2.532 Å, the distances in the oblique directions are slightly contracted to 2.235 Å, and the

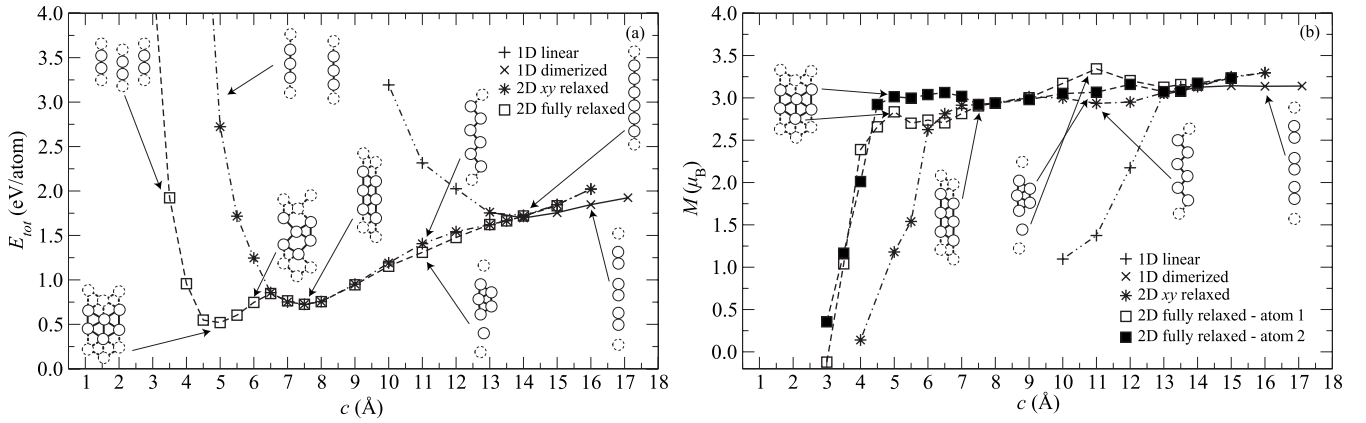


FIG. 2. Variation (a) in the total energy and (b) in the magnetic moment in one- and two-dimensional Fe nanostructures with the height of the repeat cell. Energies are measured relative to the lowest-energy configuration found for a 3D nanorod (cf. text).

angle in this isosceles triangle is  $69^\circ$ . The magnetic moment at equilibrium is  $2.92\mu_B$ . If the constraint of equal interatomic spacing along the  $z$  direction is lifted, we find that the transition from straight to zigzag wires does not occur via a homogeneous deformation: the formation of a triangular arrangement starts in the central part of the wire and at  $c \sim 11$  Å clustering is favored [see Figs. 1 and 2(a)]. Upon further contraction of the cell, the repeated clusters reconnect, but it is evident that the formation of a triangular pattern starts from the central part of the cell.

If the cell height is compressed below  $7.5$  Å, the triangular stripe is under compressive strain and for  $c \leq 6.5$  Å a transition to a stripe consisting of centered hexagons is initiated. Local equilibrium is achieved at  $c = 4.730$  Å—at this point the interatomic distance along the  $z$  direction is  $2.365$  Å and the distance in the oblique directions is slightly elongated to  $2.411$  Å, which is only slightly smaller than in bcc Fe. The magnetic moment is higher for the atoms at the outer edge of the stripe ( $2.92\mu_B$ ) than for the central atoms ( $2.67\mu_B$ ). The total energy is still higher by about  $0.51$  eV/atom than in a three-dimensional configuration (see below). Upon compression beyond the local equilibrium state, both the triangular and hexagonal stripes disintegrate to form separated parallel wires. The transition to a nonmagnetic

state is initiated at  $c \sim 6$  Å for the triangular and at  $c \sim 4.5$  Å for the hexagonal stripe.

### B. Nanorods

The total energies and magnetic moments of the three-dimensional nanostructures are displayed in Fig. 3. Formation of a nanorod is most easily initiated by twisting a triangular stripe (forming the “transitional” structure shown in Figs. 1 and 3), leading to the formation of a rod formed by distorted tetrahedra and square pyramids. The energy minimum for this arrangement is reached at  $c = 4.863$  Å; the energy is lower by about  $0.20$  eV/atom than in the energetically most favorable planar stripe. Close to this point, an arrangement in the form of trigonal antiprisms is energetically degenerate, but in contrast to the tetrahedral structure it allows a further compression to  $c = 3.864$  Å. Alternatively, this structure may also be viewed as a stacking of slightly distorted octahedra sharing a triangular facet perpendicular to the direction of the nanorod. At equilibrium (which defines the reference energy for all nanostructures) Fe-Fe distances in the isosceles triangle layers perpendicular to the  $z$  direction are  $2.310$  and  $2.761$  Å and Fe-Fe distances between these layers are  $2.480$  and  $2.384$  Å. We have also tested a

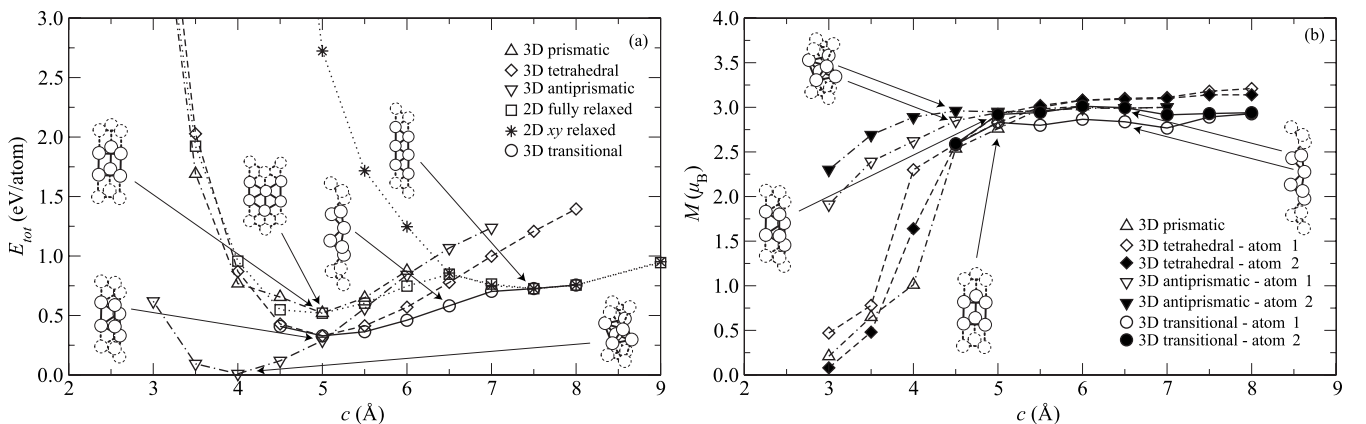


FIG. 3. Variation (a) in the total energy and (b) in the magnetic moment in two- and three-dimensional Fe nanostructures with the height of the repeat cell. Energies are measured relative to the lowest-energy configuration found for a 3D nanorod (cf. text).

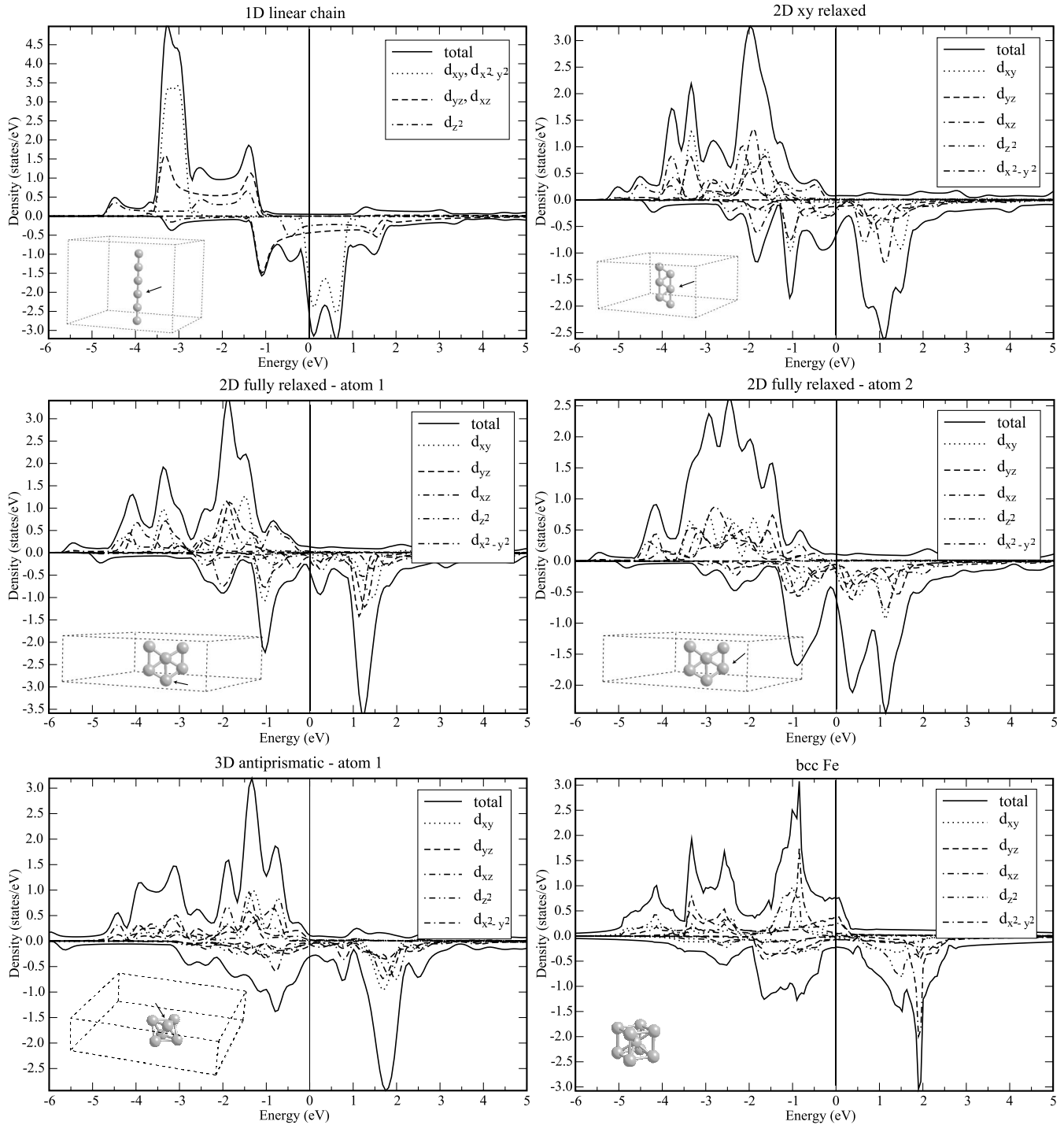


FIG. 4. Total and partial spin-polarized electronic DOSs of various Fe nanostructures in one, two, and three dimensions (see captions of the different panels), compared with the DOS of bcc Fe (cf. text).

structure formed by triangular prisms, but we find it to be the energetically least favorable structure among all 3D nanorods (see Fig. 3). It is important to emphasize that the prismatic and antiprismatic rods are not formed spontaneously upon compression of the 2D nanostructures. The antiprismatic structure is energetically degenerate with the transitional structure at  $c \sim 5 \text{ \AA}$ , but to adopt this configuration, bonds must be broken and reformed, and this is possible only by overcoming a certain potential-energy barrier. Uncon-

strained relaxation of highly compressed structures would lead to the formation of nearly planar arrangement of the six atoms in the repeat cell—but to explore realistic structures in this regime would require considerably larger models.

At equilibrium or under slight tension, the magnetic moments of the Fe atoms in the 3D nanorod range between  $2.75\mu_B$  and  $3.0\mu_B$ ; due to the distortion from the ideal reference geometry slight differences appear between inequivalent sites in the tetrahedral and antiprismatic clusters. Under

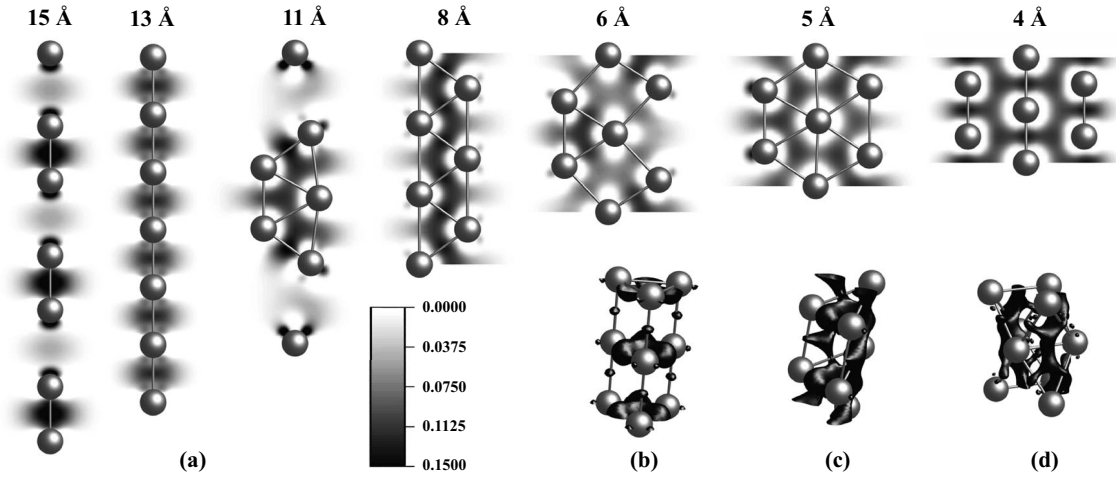


FIG. 5. (a) Contour plot of planar cuts through the difference-electron densities illustrating the chemical bonding in one- and two-dimensional nanostructures. Parts (b)–(d) show isosurfaces of the difference-electron densities in (b) prismatic, (c) tetrahedral, and (d) antiprismatic nanorods. Isosurfaces correspond to values of the difference-electron density of  $0.075 \text{ e}/\text{Å}^3$  (cf. text).

compression a transition to a low-spin state is predicted for prismatic and tetrahedral configurations at  $c \sim 4.5 \text{ Å}$ , while in the antiprismatic configuration the magnetic moment decreases only slowly.

### C. Electronic structure and binding

The changing dimensionality of the nanostructures is reflected in their electronic properties. Figure 4 shows the total and partial spin-polarized electronic densities of states (DOSs) for one-, two-, and three-dimensional arrangements. For the straight linear nanowire the DOS consists of a superposition of subbands of marked one-dimensional character with a smeared van Hove singularity at the band edges (in a strictly one-dimensional system the DOS varies as  $1/\sqrt{|E-E_b|}$  close to the band edge at  $E_b$ ). The width of the subband is largest for the  $dd\sigma$  bands formed by  $d_{z^2}$  states extended along the axis of the wire (and hybridizing with the  $ss\sigma$  band), lower for the  $dd\pi$  bands formed by the  $d_{xz}$  and  $d_{yz}$  states, and lowest for the  $dd\delta$  band formed by  $d_{xy}$  and  $d_{x^2-y^2}$  states. In the spin-polarized DOS the Fermi level falls right at the lower edge of the empty  $dd\delta$  band of the minority states and approximately at the center of the minority  $dd\pi$  band, resulting in three spin-uncompensated electrons and a magnetic moment of  $\approx 3\mu_B$ . The exchange splitting (measured by the difference in the center of gravity of the band) is slightly larger for the  $dd\delta$  ( $\Delta_\delta \approx 3.5 \text{ eV}$ ) than for the  $dd\pi$  band ( $\Delta_\pi \approx 3 \text{ eV}$ ). The ratio  $I = \Delta/M \sim 1 \text{ eV}/\mu_B$  between exchange splitting and magnetic moment is close to the universal value of the Stoner parameter  $I$  characteristic for bulk itinerant ferromagnets.<sup>38,39</sup> The analysis of the difference-electron density (defined as the difference between the self-consistent electron density of the nanostructure and a superposition of the electron densities of free atoms arranged in the same structure) illustrates the accumulation of electrons in the  $\sigma$  and  $\pi$  bonds (see Fig. 5).

The partial DOSs for planar geometries have been calculated for stripes lying in the  $x, z$  plane. In a triangular stripe the strongest contribution to the bonds parallel to the axis of

the wire comes from  $dd\sigma$  bonds between  $d_{z^2}$  and  $dd\pi$  bonds between  $d_{yz}$  states, while  $dd\sigma$  bonds between  $d_{xz}$  states form the main contribution to the transverse nearest-neighbor bonds. Again the states extending perpendicularly to the axis of the stripe form a narrow  $dd\delta$  band overlapping with the antibonding component of the  $dd\sigma$  bands. The Fermi level falls into the deep DOS minimum of the minority states formed by the bonding-antibonding splitting. Hybridization of all in-plane orbitals is rather strong—in the difference-electron densities this results in a charge redistribution which shows, in addition to the strong  $d_{yz}-d_{xz}$  ( $d_{\text{Fe-Fe}} = 2.235 \text{ Å}$ ) and weaker  $d_{z^2}-d_{z^2}$  ( $d_{\text{Fe-Fe}} = 2.532 \text{ Å}$ ) two-electron  $\sigma$  bonds, the incipient formation of three-center bonds. The three-center bonds are most pronounced in the clusters formed at  $c \sim 11 \text{ Å}$  upon unconstrained relaxation. In a regular triangular stripe bonding is based on strong oblique two-center and three-center bonds, while the bonds parallel to the edges of the stripe are comparatively weak (see Fig. 5).

Hybridization between all in-plane  $d$  orbitals is strong in hexagonal atomic stripes. Here one has to differentiate between atoms located at the outer edge and in the central atomic row of the stripe—for the latter the bonding-antibonding splitting is much more pronounced. The stability of this geometry is reflected by the position of the Fermi level in a deep minimum of the DOS of the minority bands. The difference-electron density shows that bonding is based on the formation of three-center bonds in the basic Fe triangles. The transition from two- to three-center bonds is also illustrated in the transition structure between the triangular and hexagonal stripes (see Fig. 5).

For the three-dimensional nanorods we show the DOS only for the antiprismatic configuration. The preference for the antiprismatic rods is reflected in a stronger bonding-antibonding splitting than for the other geometries and by the location of the Fermi level in a broad and deep DOS minimum of the minority-spin states. The isosurface difference-electron density distributions are shown for the “tetrahedral,” prismatic, and antiprismatic configurations. The difference-electron densities for the antiprismatic rod show charge ac-

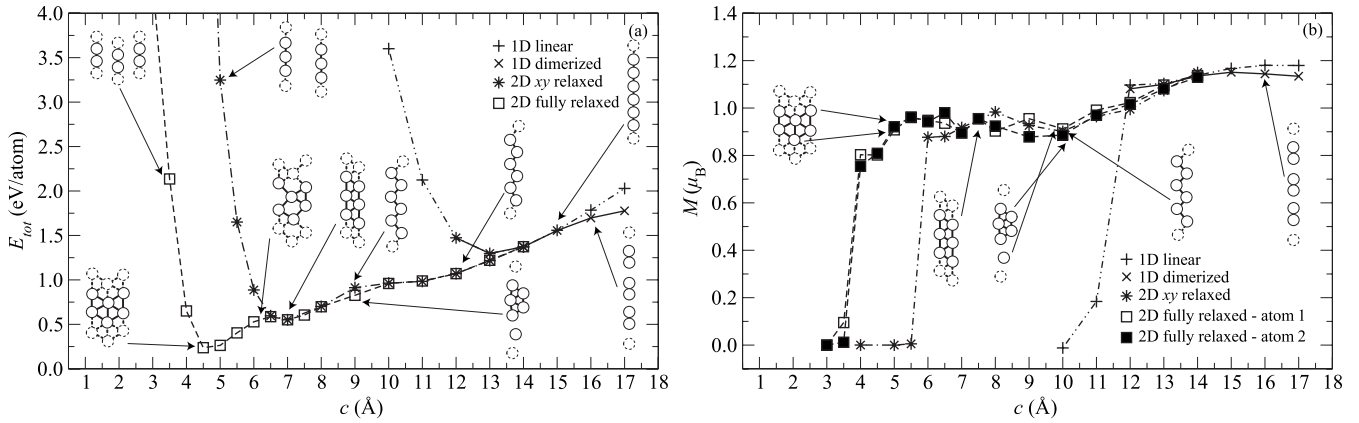


FIG. 6. Variation (a) in the total energy and (b) in the magnetic moment in one- and two-dimensional Ni nanostructures with the height of the repeat cell. Energies are measured relative to the lowest-energy configuration found for a 3D nanorod (cf. text).

cumulation in the midpoints of two-center bonds, reaching into the center of all triangular facets. In the prismatic arrangement the bonding is distinctly stronger within the triangular facets than along the all edges. Also in tetrahedral rod the highest difference-electron densities are accumulated along the nearest-neighbor bonds (perpendicular to the  $z$  axis) and reaching into the center of each tetrahedron.

#### IV. Ni NANOSTRUCTURES

##### A. Geometric structures under varying tension

The binding energies, nearest-neighbor distances, and magnetic moments of Ni nanostructures in local equilibrium are gain compiled in Table I. The nearest-neighbor distances are significantly smaller than in fcc bulk Ni, the magnetic moments are strongly enhanced to up to  $1.11\mu_B$ , for the three-dimensional nanostructures the values approach those calculated for the more open Ni(100) and Ni(110) surfaces ( $M=0.76\mu_B$ ).<sup>40</sup>

The variation in the geometric structures of the Ni nanostructures follows essentially the same pattern as described above for Fe, albeit with some significant differences (see Fig. 6). For a straight monowire, the equilibrium interatomic distance is  $2.181 \text{ \AA}$  ( $c=13.086 \text{ \AA}$ ). The magnetic moment is  $1.11\mu_B$  (compared to  $0.61\mu_B$  in bulk fcc). Under even a

slight tensile strain, the wire breaks up, forming  $\text{Ni}_2$  dimers with a Ni-Ni distance of  $2.10 \text{ \AA}$  and a magnetic moment of  $1.10\mu_B/\text{Ni}$  atom, which is in good agreement with the previously published results for Ni dimers.<sup>41</sup> Even in the equilibrium configuration, a straight linear chain is energetically slightly less favorable (by about  $66 \text{ meV/atom}$ ) than a zigzag chain. Relaxation in two dimensions under the constraint of equal distances along the  $z$  direction leads to the formation of a triangular stripe reaching an energy minimum at  $c=6.916 \text{ \AA}$  (with Ni-Ni distances of  $2.305$  and  $2.317 \text{ \AA}$ , respectively, and a bond angle of  $60^\circ$ ). In this state the magnetic moment is slightly reduced to  $0.92\mu_B$ . As for Fe, the transition from a wire to a stripe does not occur by a homogeneous deformation, clustering is energetically favored at intermediate cell height (see Fig. 6). A modest compression of the triangular stripe induces a transition to a broader stripe with the Ni atoms forming centered hexagons. Equilibrium is reached at  $c=4.702 \text{ \AA}$ , with a magnetic moment of  $0.88\mu_B$ . Both one-dimensional wires and two-dimensional stripes undergo an abrupt transition to a nonmagnetic state upon modest compression. The critical value of the interatomic distance is  $d \sim 1.9\text{--}2.0 \text{ \AA}$  for both wires and stripes.

The transition to a three-dimensional rod is illustrated in Fig. 7. If a full relaxation of all coordinates is admitted, the planar triangular stripe is found to be instable against the formation of a transition configuration consisting of alternat-

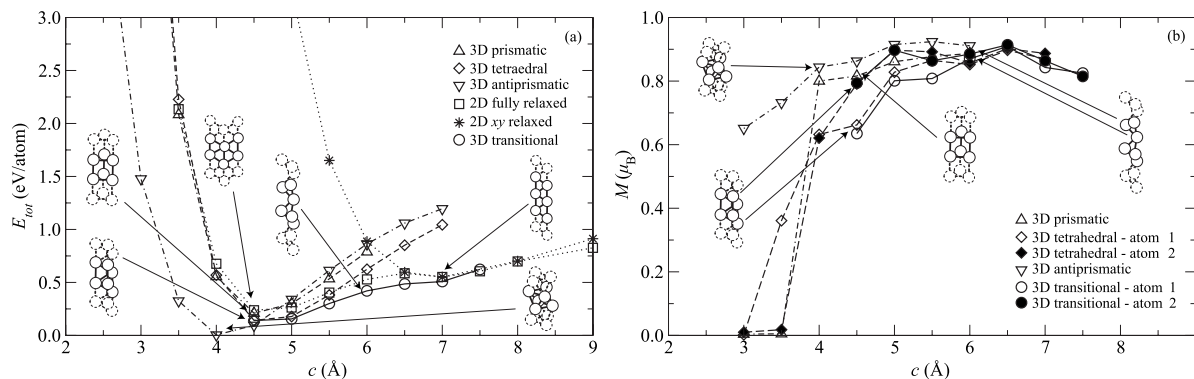


FIG. 7. Variation (a) in the total energy and (b) in the magnetic moment in two- and three-dimensional Ni nanostructures with the height of the repeat cell. Energies are measured relative to the lowest-energy configuration found for a 3D nanorod (cf. text).

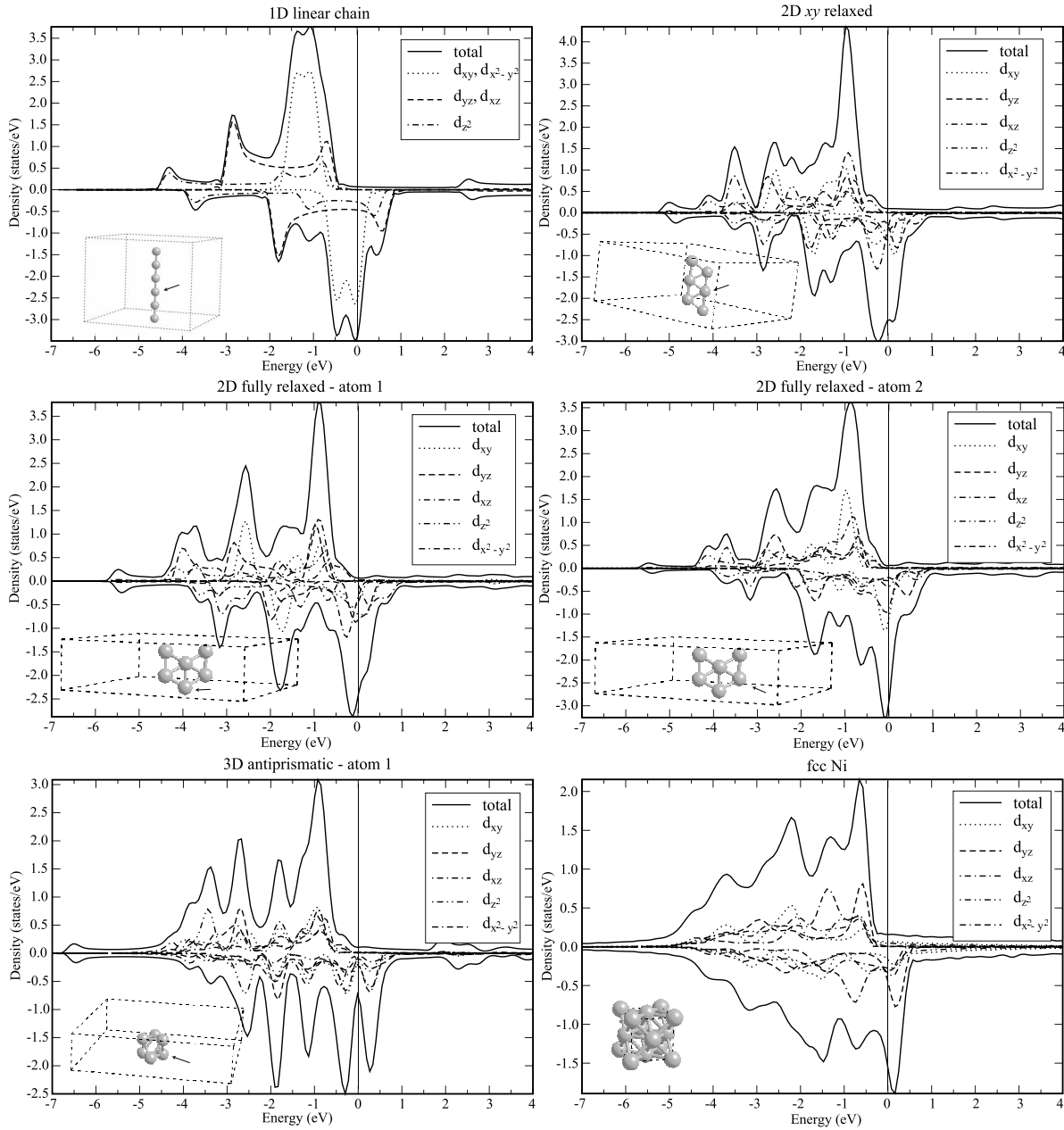


FIG. 8. Total and partial spin-polarized electronic DOSs of various Ni nanostructures in one, two, and three dimensions (see captions of the different panels), compared with the DOS of bcc Ni (cf. text).

ing edge- and corner-sharing triangles leading to a structure consisting of face-sharing tetrahedra and square pyramids (“3D tetrahedral”). This arrangement may also be viewed as resulting from a shearing of the two triangular faces of a prism. Rotation of the two triangles finally leads to the most stable antiprismatic (or octahedral) arrangement of the Ni atoms in the nanorod. In contrast to Fe at equilibrium ( $c = 4.076 \text{ \AA}$ ) the antiprismatic structure consists of equilateral triangles perpendicular to the axis of the rod, with Ni-Ni distances of  $2.223 \text{ \AA}$ . The distance between Ni atoms in different triangles is  $2.416 \text{ \AA}$ . The structural energy differences relative to the tetrahedral and prismatic rods are about a factor of 2 smaller than for Fe. At equilibrium, the magnetic moments in all 3D configurations are about  $0.85\mu_B$ . Even a

modest compression causes the collapse of the magnetic moments in the prismatic and tetrahedral structures starting at  $c \sim 4 \text{ \AA}$  ( $d \sim 2 \text{ \AA}$ ), while in the antiprismatic configuration the magnetic moment decreases only gradually.

### B. Electronic structure and binding

Our results for the spin-polarized partial DOSs of the Ni nanostructures are compiled in Fig. 8. While the general trends are similar as for the Fe nanostructures discussed above, we also observe some characteristic differences. For the linear chain the narrow  $dd\delta$  band is up shifted relative to the broader subbands; the Fermi level falls in the region of the highest DOS of the minority states. In both Fe and Ni

nanowires the states at the Fermi edge are nearly completely spin polarized. In the Ni wire, the exchange splitting is reduced to about 1.1 eV such that the value of the Stoner parameter is again close to the universal value of  $I=\Delta/M \sim 1 \text{ eV}/\mu_B$ . The electronic DOSs of both triangular and hexagonal stripes are characterized by a three-peaked structure associated with the  $\sigma$  bonds formed by  $d_{z^2}$  and  $d_{xz}$  orbitals,  $\pi$  bonds formed by  $d_{yz}$  orbitals, and  $\delta$  bonds formed by the  $d_{xy}$  and  $d_{x^2-y^2}$  states. Especially for the minority states this structure is more pronounced than for the Fe stripes. A strongly structured DOS is also calculated for the 3D nanorods. The energetic preference for the antiprismatic rod is evidently promoted by the location of the Fermi level in a deep DOS minimum of the minority DOS. Note that for both metals, the DOS of the antiprismatic nanorod already approaches the spectrum of the bulk metals: for Fe we observe a strong bonding-antibonding splitting of the band like in the bcc metal. For Ni, the splitting is strongly reduced, and the DOS approaches the antisymmetric shape characteristic for a fcc metal.

## V. CONCLUSIONS

We have presented detailed spin-density functional studies of the magnetic properties in low-dimensional nanostructures of Fe and Ni, ranging from straight linear wires over planar stripes to three-dimensional nanorods. With decreasing tension on the system, the configuration changes from a dimerized to a periodic linear chain over a zigzag chain first to a planar triangular stripe and further to a three-dimensional rod. These rods consist first of twisted arrange-

ment of corner- and face-sharing triangles and finally of a periodic stacking of antiprismatic units. Ni nanostructures tend to assume slightly more regular geometries. For example, the triangular facets of the Ni antiprisms are equilateral triangles, while the Fe antiprisms are formed by isosceles triangles.

In all nanostructures, Fe and Ni atoms are in a high-spin state with almost constant magnetic moments of  $3.0\mu_B \rightarrow 3.1\mu_B$  for Fe and  $0.9\mu_B \rightarrow 1.0\mu_B$  for Ni. Independently of the dimensionality of the nanostructure and the coordination number, a transition from this high-spin to a low-spin or nonmagnetic state is initiated at a critical interatomic distances of  $2.1 \rightarrow 2.2 \text{ \AA}$  for Fe and  $1.9 \rightarrow 2.0 \text{ \AA}$  for Ni. Note, however, that at these critical distances the low-dimensional structures are already energetically less favorable than a structure with a higher dimension. The analysis of the electronic densities of states shows that the ratio between the exchange splitting (as measured by the difference in the positions of the center of gravity of the spin-up and spin-down bands) and the magnetic moment is independent of the dimensionality of the nanostructure and equals the universal value  $I=\Delta/M \sim 1 \text{ eV}/\mu_B$  derived for bulk itinerant magnets.

## ACKNOWLEDGMENTS

This work was supported by the Austrian Science Funds under Project No. P19712-NO, by the Academy of Sciences of the Czech Republic under Research Project No. AV0Z20410507, and by the Ministry of Education of the Czech Republic under Research Project No. MSM0021622410.

- 
- <sup>1</sup>N. D. Mermin and H. Wagner, Phys. Rev. Lett. **17**, 1133 (1966).  
<sup>2</sup>P. Gambardella, M. Blanc, H. Brune, K. Kuhnke, and K. Kern, Phys. Rev. B **61**, 2254 (2000).  
<sup>3</sup>D. Spišák and J. Hafner, Phys. Rev. B **65**, 235405 (2002).  
<sup>4</sup>H. Ohnishi, Y. Kondo, and K. Takayanagi, Nature (London) **395**, 780 (1998).  
<sup>5</sup>A. I. Yanson, G. Rubio Bollinger, H. E. van den Broom, N. Agrait, and J. M. van Ruitenbeek, Nature (London) **395**, 783 (1998).  
<sup>6</sup>G. Rubio, N. Agrait, and S. Vieira, Phys. Rev. Lett. **76**, 2302 (1996).  
<sup>7</sup>V. Rodrigues, J. Bettini, P. C. Silva, and D. Ugarte, Phys. Rev. Lett. **91**, 096801 (2003).  
<sup>8</sup>S. R. Bahn and K. W. Jacobsen, Phys. Rev. Lett. **87**, 266101 (2001).  
<sup>9</sup>P. Velez, S. A. Dassie, and E. P. M. Leiva, Chem. Phys. Lett. **460**, 261 (2008).  
<sup>10</sup>I. Tsetseris and S. T. Pantelides, Mater. Sci. Eng., B **152**, 109 (2008).  
<sup>11</sup>R. Inguanta, S. Piazza, and C. Susseria, Electrochim. Acta **53**, 5766 (2008).  
<sup>12</sup>Y. P. Han, H. A. Ye, W. Z. Hu, and G. Shi, Mater. Lett. **62**, 2806 (2008).  
<sup>13</sup>S. Liu, X. Tang, Y. Mastai, I. Felner, and A. Gedanken, J. Mater. Chem. **10**, 2502 (2000).  
<sup>14</sup>N. Grobert, W. K. Hsu, Y. Q. Zhu, J. P. Hare, H. W. Kroto, D. R. M. Walton, M. Terrones, H. Terrones, R. Redlich, M. Rühle, R. Escudero, and F. Morales, Appl. Phys. Lett. **75**, 3363 (1999).  
<sup>15</sup>D. Spišák and J. Hafner, Phys. Rev. B **67**, 214416 (2003).  
<sup>16</sup>C. Ederer, M. Komelj, and M. Fähnle, Phys. Rev. B **68**, 052402 (2003).  
<sup>17</sup>J. Hong and R. Q. Wu, Phys. Rev. B **67**, 020406(R) (2003).  
<sup>18</sup>A. Delin and E. Tosatti, Phys. Rev. B **68**, 144434 (2003).  
<sup>19</sup>D. Sanchez-Portal, E. Artacho, J. Junquera, A. Garcia, and J. M. Soler, Surf. Sci. **482-485**, 1261 (2001).  
<sup>20</sup>P. Sen, S. Ciraci, A. Buldum, and I. P. Batra, Phys. Rev. B **64**, 195420 (2001).  
<sup>21</sup>F. J. Ribeiro and M. L. Cohen, Phys. Rev. B **68**, 035423 (2003).  
<sup>22</sup>Lin Yi-Shou, Li Ai-Yu, and Zhu Zi-Zhong, Chin. Phys. Lett. **21**, 1791 (2004).  
<sup>23</sup>A. Y. Li, R. Q. Li, Z. Z. Zhu, and Y. H. Wen, Physica E (Amsterdam) **30**, 138 (2005).  
<sup>24</sup>J. C. Tung and G. Y. Guo, Phys. Rev. B **76**, 094413 (2007).  
<sup>25</sup>C. Ataca, S. Cahangirov, E. Durgun, Y. R. Jang, and S. Ciraci, Phys. Rev. B **77**, 214413 (2008).  
<sup>26</sup>C. Jo and J. I. Lee, J. Magn. Magn. Mater. (unpublished).  
<sup>27</sup>G. Kresse and J. Furthmüller, Phys. Rev. B **54**, 11169 (1996); Comput. Mater. Sci. **6**, 15 (1996).

- <sup>28</sup>P. E. Blöchl, Phys. Rev. B **50**, 17953 (1994).
- <sup>29</sup>G. Kresse and D. Joubert, Phys. Rev. B **59**, 1758 (1999).
- <sup>30</sup>J. P. Perdew, K. Burke, and M. Ernzerhof, Phys. Rev. Lett. **77**, 3865 (1996).
- <sup>31</sup>E. G. Moroni, G. Kresse, J. Hafner, and J. Furthmüller, Phys. Rev. B **56**, 15629 (1997).
- <sup>32</sup>P. Villars and L. D. Calvert, *Pearson's Handbook of Crystallographic Data for Intermetallic Phases*, 2nd ed. (ASM International, Metals Park, OH, 1991).
- <sup>33</sup>Y. Tsunoda, J. Phys.: Condens. Matter **3**, 7231 (1991).
- <sup>34</sup>M. Marsman and J. Hafner, Phys. Rev. B **66**, 224409 (2002).
- <sup>35</sup>D. Qian, X. F. Jin, J. Barthel, M. Klaua, and J. Kirschner, Phys. Rev. Lett. **87**, 227204 (2001).
- <sup>36</sup>D. Spišák and J. Hafner, Phys. Rev. B **66**, 052417 (2002).
- <sup>37</sup>P. Blonski, A. Kiejna, and J. Hafner, Surf. Sci. **590**, 88 (2005).
- <sup>38</sup>F. J. Himpsel, Phys. Rev. Lett. **67**, 2363 (1991).
- <sup>39</sup>I. Turek, Ch. Becker, and J. Hafner, J. Phys.: Condens. Matter **4**, 7257 (1992).
- <sup>40</sup>F. Mittendorfer, A. Eichler, and J. Hafner, Surf. Sci. **423**, 1 (1999).
- <sup>41</sup>T. Futschek, J. Hafner, and M. Marsman, J. Phys.: Condens. Matter **18**, 9703 (2006).